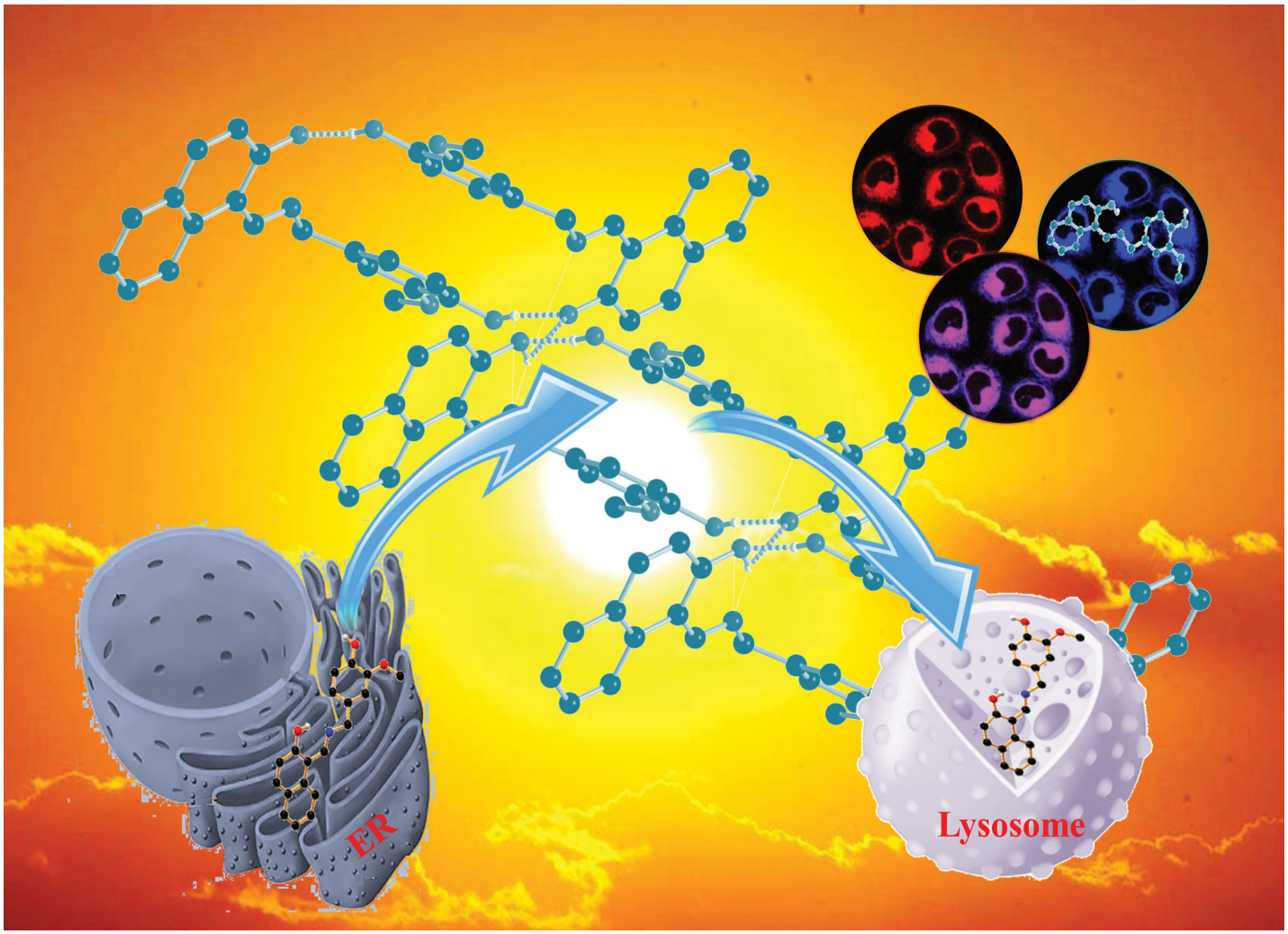

Showcasing research from Dr Shaikh M. Mobin's group, Discipline of BSBE and Chemistry at Indian Institute of Technology Indore, India. Image designed by Ms Pratibha Kumari and Mr Sanjay K. Verma

A facile two-photon fluorescent probe: an endoplasmic reticulum tracker monitoring ER stress and vesicular transport to lysosomes

Various human diseases are associated with improper vesicle transport from the Endoplasmic Reticulum (ER) to various organelles. The present fluorescent probe selectively labels the ER in live cells and monitors vesicle transport from the ER to the lysosome in real time.

As featured in:

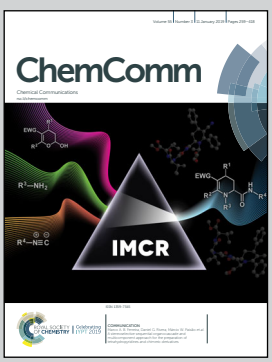

See Shaikh M. Mobin *et al.*, *Chem. Commun.*, 2019, **55**, 294.

ROYAL SOCIETY OF CHEMISTRY | Celebrating IYPT 2019

rsc.li/chemcomm

Registered charity number: 207890

ChemComm

COMMUNICATION

View Article Online
View Journal | View Issue

Cite this: *Chem. Commun.*, 2019, 55, 294

Received 14th September 2018,
Accepted 7th November 2018

DOI: 10.1039/c8cc07429a

rsc.li/chemcomm

A facile two-photon fluorescent probe: an endoplasmic reticulum tracker monitoring ER stress and vesicular transport to lysosomes†

Pratibha Kumari,[a] Sanjay K. Verma[b] and Shaikh M. Mobin*[abc]

The morphological divergence of the Endoplasmic Reticulum (ER) during stress is a powerful indicator of several diseases. A new two-photon, non-cytotoxic, fluorescent probe (ERLp) was designed and synthesized in a facile manner for selective tracking of the Endoplasmic Reticulum (ER) with a high Pearson co-localization coefficient (0.91) in live cells and tumor spheroids. Further, ER stress during cell apoptosis and vesicular transport from the ER to the lysosomal compartment were also explored by employing ERLp. Therefore, ERLp can be used as a potent tool for examining vesicle transport or ER stress associated diseases in real time.

The Endoplasmic reticulum (ER) plays an important role in various biological processes such as synthesis, proper folding, modification of proteins and their trafficking to other organelles. It also regulates intracellular calcium ions and lipid metabolism.[1] With the help of vesicles, intracellular movement of constituents is carried out between different cell organelles.[2] Transport of materials to specific organelles depends on the target motifs of the transported proteins, conformational variation and chemical modifications.[3] Various human diseases are caused by the improper function of the vesicle transport process, including Alzheimer's disease,[4] and several associated genetic disorders such as Niemann–Pick disease type C,[5] Lafora disease,[6] and Tay–Sachs disease.[7]

The ER is extremely sensitive to stress, which causes aggregation and accumulation of unfolded proteins.[8] Since protein aggregation is harmful to cells, ER stress leads to various pathological conditions, which include stroke, heart disease, neurodegenerative diseases, ischaemia, diabetes, and cancer.[9] For imaging of the ER, various fluorescent probes have been developed, such as $DiOC_5(3)$, $DiOC_6(3)$ and hexyl rhodamine B.[10] Nevertheless, these probes have some limitations like low selectivity, poor photo-stability, non-specific localization to other organelles and broad emission spectrum insensitivity.[11] The green fluorescent protein (GFP) fusion technology, which is commonly used for monitoring vesicle transport, is restricted to living organisms[12] due to the fact that artificial fusion gene transfection requires hostile conditions,[13] which can alter the organisms' cellular metabolism.[14] Cells expressing GFP undergo oxidative stress[15] and apoptosis.[14] Thus, a consistent fluorescent ER targeting probe that monitors vesicular transport should exhibit ER selective localization, a narrow emission spectrum, photostability, high cell viability and display two-photon excited fluorescence. Two-photon microscopy (TPM) is an attractive instrument for live cell and tissue imaging where the fluorophore gets excited by two near-infrared photons (>700 nm). This technique has numerous advantages over one-photon microscopies such as low phototoxicity to cells, negligible background interference, limited photobleaching and a deep penetration depth (>500 μm).[16] Therefore, TPM is a significant device for bio-imaging within living tissue or cells and is rarely explored in small molecules.[16b]

The probes reported so far for endoplasmic reticulum imaging are generally based on one-photon microscopy based on rhodol analogs, complex organic fluorophores and metal-complexes (Chart S1, ESI†), which involves multi-step tedious synthetic routes.[1a,11b,c,17]

Herein, we report the design and facile synthesis of an Endoplasmic Reticulum to Lysosome probe (**ERLp**) with sharp fluorescence emission and high photostability in a biological system which tracks the ER and monitors ER dynamics under ER stress conditions and vesicular transport from the ER to the lysosome. **ERLp** was synthesized by the simple condensation reaction of 2-hydroxy-1-naphthaldehyde with 4-(aminomethyl)-2-methoxyphenol hydrochloride in methanol at room temperature, resulting in a light brown solid in 92% yield (Scheme 1). **ERLp** was well characterized by ^{1}H, ^{13}CNMR, FTIR and mass spectroscopy (Fig. S1–S4, ESI†), and for chemical stability in solution, the ^{1}H NMR spectrum of **ERLp** was recorded after

[a] *Discipline for Biosciences and Bio-Medical Engineering, Indian Institute of Technology Indore, Simrol Indore 453552, India*
[b] *Discipline of Chemistry, Indian Institute of Technology Indore, Simrol Indore 453552, India*
[c] *Discipline of Metallurgical Engineering and Material Science, Indian Institute of Technology Indore, Simrol Indore 453552, India. E-mail: xray@iiti.ac.in*

† Electronic supplementary information (ESI) available. CCDC 1854514. For ESI and crystallographic data in CIF or other electronic format see DOI: 10.1039/c8cc07429a

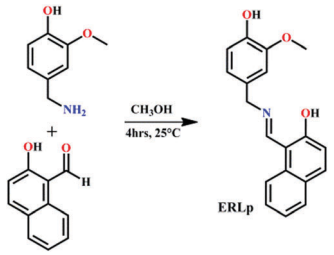

Scheme 1 Schematic representation of the synthesis of **ERLp**.

2 days in DMSO-d_6 solution at 25 °C and found to be stable (Fig. S5, ESI†). **ERLp** was further authenticated by single crystal X-ray diffraction study. A single crystal of **ERLp** was grown by slow evaporation of methanol solution at 25 °C and crystallized in a monoclinic crystal system with the centrosymmetric $P21/n$ space group (Tables S1, S2 and Fig. S6, ESI†).[18] The non-planar crystal structure of **ERLp** is due to the presence of the naphthyl and methoxy phenolic rings in two different planes *via* the imine (>C=N–) unit, with a torsion angle of 70.62°. The packing features of **ERLp** reveal the formation of supramolecular 3D-architecture along the *b*-axis, which was further stabilized by π···π stacking interactions (3.931 Å) between the two phenyl rings of the different moieties in a tail-to-tail arrangement (ESI,† Fig. S7–S10).

To examine the photo-physical behaviour of **ERLp**, absorption and emission spectra were recorded in acetonitrile solution (Fig. S11, ESI†). **ERLp** exhibits an absorption band at 230 nm, which corresponds to π → π*, which indicates the presence of the aromatic moiety, whereas the bands at 306, 400 and 419 nm are due to n → π* because of the presence of hetero-atoms. Further, a strong and sharp emission band at 423 nm was observed in the fluorescence spectrum of **ERLp** in acetonitrile solution (Fig. S11, ESI†), but in PBS (Phosphate Buffer Saline) it shows a slightly hypochromic-shift as compared to the acetonitrile solution; this may be due to the presence of the hydrophobic methoxy group in **ERLp** (Fig. S12, ESI†). Moreover, the fluorescence intensity of **ERLp** was measured at different pHs (pH 9.45–4.14), which shows that the fluorescence signal is almost stable (Fig. S13, ESI†). The two-photon fluorescence intensity was confirmed at 740 nm (Fig. S14 and S15, ESI†).

The excellent photo-physical properties and highly fluorescent nature of **ERLp** prompted us to explore cell activities by employing **ERLp**. The probe **ERLp** was found to be biocompatible as it does not interfere in cell proliferation up to a tested concentration of 140 μM for 24 h as confirmed by MTT assay (Fig. S16, ESI†).

For profound cell activities, flow cytometry and fluorescence microscopy techniques were introduced, which provide data of single-cell analysis. Flow cytometry provides high-quality fluorescence signals from large populations of cells in flow (suspension cells), whereas fluorescence microscopy provides detailed evidence of the target morphology in small sample sizes.[19] Hence, fluorescence imaging analysis was done by flow cytometry. The mean fluorescence intensity of control cells (unstained cells) corresponds to 70 and those of **ERLp** treated cells with 40 μM and 80 μM were found to be 1141 and 1772, respectively, which leads to the movement of a huge population of cells towards the right with respect to the control (Fig. S17, ESI†). This reveals that **ERLp** can uniformly label a huge population of cells.

Concentration dependent live cell staining was performed with **ERLp**. As the time of incubation is increased from 10 min to 2 h, staining is possible even at low concentrations up to 5 μM (Fig. S18 and S19, ESI†). The **ERLp** concentration used for the cellular experiment is higher than that of the standard ER tracker due to the lower quantum yield of **ERLp** (12%) than the commercial ER Tracker Red (Table S3, ESI†).[20]

The photostability of the ER tracking marker is an important parameter for long-term bio-imaging during morphological and physiological changes or ER stress study. Thus, an **ERLp** photobleaching experiment was performed both in solution and in live cells. An aqueous solution of **ERLp** was continuously UV illuminated (254 nm) at 25 °C, and no drastic change in the fluorescence intensity of **ERLp** was observed up to 80 min (Fig. S20, ESI†). Further **ERLp** and ER Tracker Red were explored for the photobleaching experiment using HeLa cells. The result indicates that the two-photon fluorescence intensity of **ERLp** after 1800 scans is retained at an impressive 64%, whereas the fluorescence intensity of ER Tracker Red after 1800 scans diminished to 28% (Fig. S21 and Movies S1, S2, ESI†). Photostability was high in the cells due to the visible light range wavelength used in confocal microscopy, whereas the infrared light region is used in two photon microscopy. Thus, **ERLp** shows high photo-stability for long-term live cell imaging.

In order to confirm the intracellular specific localization of **ERLp**, co-localization experiments were conducted with **ERLp** and various commercially available organelle trackers such ER, lysosome and mitochondria trackers (Fig. S22, ESI†). The Pearson colocalization coefficient of **ERLp** with an ER tracker was found to be 0.86, whereas the colocalization coefficients for **ERLp** with lyso and mito trackers were 0.69 and 0.46, respectively (Fig. S22, ESI†), thus indicating that **ERLp** specifically localized in the endoplasmic reticulum with a high Pearson coefficient.

Further, the selective staining capability of **ERLp** towards the universal Endoplasmic Reticulum (ER) was evaluated on various cell lines such as cervical cancer (HeLa), prostate cancer (DU145), skin melanoma (A375) and breast cancer (MCF-7) cells (Fig. S23, ESI†). **ERLp** shows an excellent ER labeling pattern in all the studied cell lines. Additionally, the co-localization result of **ERLp** and ER-Tracker Red was calculated using the Pearson co-localisation coefficient (R_r) (Fig. S24, ESI†). To our surprise, the super-imposed fluorescent pink signals (blue and red) exhibited high Pearson coefficients of 0.87, 0.88, 0.85 and 0.84 for HeLa, DU145, A375 and MCF-7 cells, respectively.

Two-photon microscopy (TPM) live cell imaging is a superior technology to one photon imaging in terms of its low background signal, low photo-damage, and large depth imaging (>500 μm).[21] However, to compare both one and two-photon microscopies, co-localization imaging was performed for **ERLp** with ER Tracker Red, which validates excellent superimposition in both cases with a very high Pearson colocalization coefficient

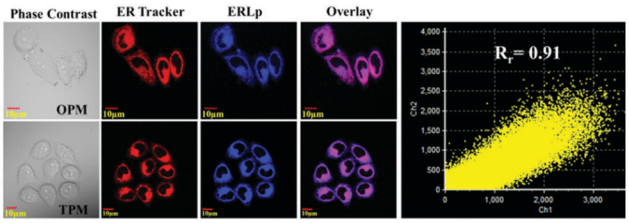

Fig. 1 One-photon microscopy (OPM) and two-photon microscopy (TPM) images of live HeLa cells. Cells were co-stained with **ERLp** (80 μM, 10 min) and ER Tracker Red (1 μM, 30 min). **ERLp**: λ_{ex} = 405 nm (OPM) or 740 nm (TPM). ER Tracker Red, λ_{ex} = 559 nm (OPM). The images were taken under a 60× 2z oil immersion objective, scale bar 10 μm.

of 0.91 (Fig. 1). To the best of our knowledge, this is the best among the so far reported ER probes.[17c,22]

ER stress is triggered by various conditions that interrupt the proper folding of proteins in the ER.[23] After confirming the role of **ERLp** as an ER tracker, we decided to further explore the possibility whether **ERLp** is capable of monitoring ER stress. Thus, to emphasize tracking of ER stress during apoptosis, cells were treated with tunicamycin, which blocks N-linked glycosylation of newly synthesized proteins, or dithiothreitol (DTT, a strong reducing agent), which blocks disulfide-bond formation in proteins, and consequently induces ER stress causing various misfolded proteins in the ER. After addition of tunicamycin (40 μg ml^{-1}) or DTT (200 μM), the red colour stain of ER Tracker Red starts disappearing after 1 h; this implies that the ER is under stress and apoptosis is initiated. Subsequently, the cell morphology starts changing. The fluorescence intensity of ER Tracker Red diminishes as cells undergo stress, but **ERLp** remains fluorescent and tracks ER stress during apoptosis (Fig. 2 and Fig. S25 and S26, ESI†). Thus, it can be concluded that **ERLp** is capable of monitoring dynamic changes in the ER membrane during stress conditions. Possibly, **ERLp** may provide a useful tool for examining ER dynamics.

ERLp gradually shifted from the ER to a granular shape within 90 minutes as shown in time course TPM images (Fig. 3a). Therefore, the time-dependent Pearson colocalization (R_r) values were monitored from the colocalization experiments of **ERLp** with ER Tracker Red and lysosome tracker red

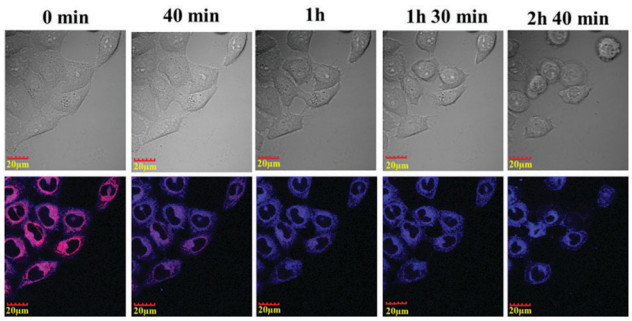

Fig. 2 Endoplasmic reticulum stress leads to cell apoptosis. Here HeLa cells were labeled with **ERLp** (80 μM, 10 min) and co-stained with ER Tracker Red (1 μM, 30 min), then tunicamycin (40 μg ml^{-1}) was added and the image was captured after a different time interval. (Here only the overlay images are shown for simplicity.) Scale bar 20 μm.

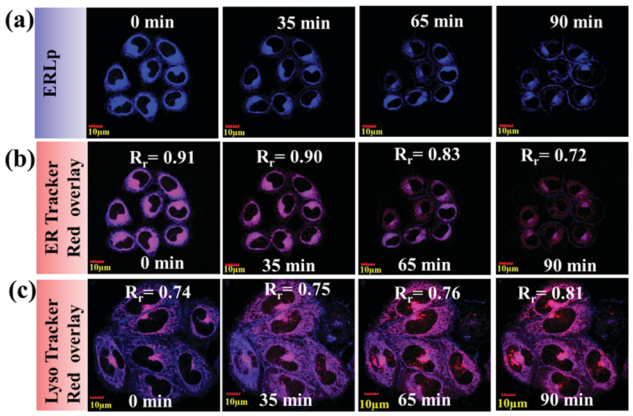

Fig. 3 (a) Time-dependent TPM images of live HeLa cells stained with **ERLp**, (b) HeLa cells stained with **ERLp** and co-labeled with ER Tracker Red, and (c) HeLa cells stained with **ERLp** and co-labeled with Lyso Tracker Red DND-99. (In the case of b and c only the overlay images are displayed for clarity.) Scale bars = 10 μm.

(Fig. 3b, c and Fig. S27, S28, ESI†). The R_r (co-localization) value of **ERLp** towards the ER tracker gradually decreases from 0.91 to 0.72, whereas the R_r value towards lysosome tracker slowly increases from 0.74 to 0.81. These results demonstrate the dual nature of **ERLp**, initially restricted to the ER and then slowly transported from the ER to lysosomes. This may be associated with the ER to the lysosome vesicle transport system.

In comparison with 2D cell monolayer culture, 3D tumor spheroids mimic numerous *in vivo* features of solid tumors, such as cell–cell interactions, spatial architecture, hypoxia, physiological responses, gene expression patterns and drug penetration mechanisms. Thus, the cell morphology closely resembles its natural pattern in the human physiological system.[19]

The imaging of deeper layers of tumor spheroids through a confocal microscope still has so many technical challenges. To address this issue, two different size spheroids were incubated with **ERLp** for imaging. The images were captured after every 2 μm section cutting along the *Z*-axis. The two-photon excitation showed much deeper and uniform penetration of **ERLp** up to ~94 μm as compared to one-photon excitation, where the penetration was up to ~42 μm (Fig. 4, Fig. S29 and S30 and Movies S3, S4 and, S5, ESI†). The results concluded that the spheroids exhibited stronger fluorescence in deeper layers, signifying the enhanced penetrating power of two-photon excitation light. Thus, **ERLp** may be further exploited for its application in *in vivo* endoplasmic reticulum imaging in living organs or tissue.

The probable mechanistic pathway of **ERLp** uptake was determined by confocal microscopy. For this purpose, HeLa cells were treated with **ERLp** in two separate dishes: one of them incubated at 4 °C and the other at 37 °C, in order to diagnose ligand uptake by the cells *via* an energy-independent or energy-dependent pathway. The **ERLp** uptake by live cells at 4 °C as well as 37 °C demonstrates that the uptake is through an energy-independent pathway (Fig. S31, ESI†). To explain the dual role of **ERLp** as an ER tracker and subsequently with time as a lysosome tracker, a two-photon excitable probe was designed by

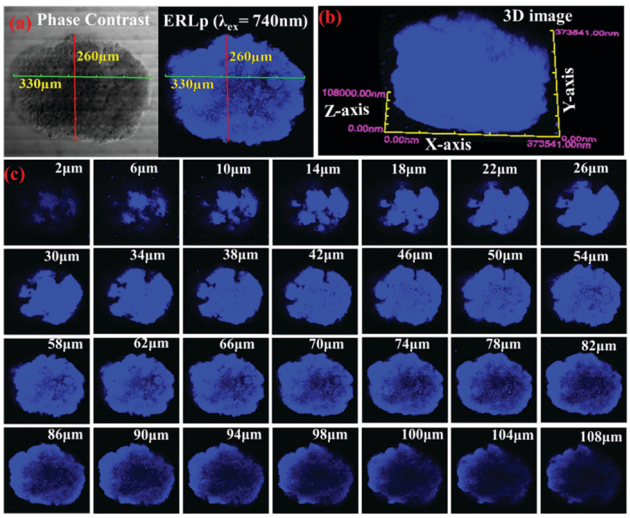

Fig. 4 (a) Two-photon fluorescence images of the 1st multicellular tumor spheroid after **ERLp** treatment (80 μM, for 1 h). (b) The Z-stack 3D image of the tumor spheroid. (c) Z-stack images were taken from the top to bottom of a spheroid, after every 2 μm section cutting. The images were taken under a 20× 1.7z objective; λ_{ex} = 740 nm; λ_{em} = 415–470 nm.

introducing (i) an imine group at position 1 of β-hydroxy-naphthalene and (ii) an ortho methoxyphenol unconjugated unit, which leads to a push–pull of **ERLp** from the ER to lysosomes. The pK_a value plays a decisive role in controlling the movement of the probe inside the cell.[24] The remote phenolic hydroxyl group of **ERLp** is responsible for the ER tracking; this may be due to the hydrophobic nature of this group having a pK_a value of 9.9 (Fig. S32, ESI†). On the other hand, the presence of the imine having a low pK_a value of 3.9 and the naphthyl hydroxyl group of **ERLp** in a conjugated manner with a hydrophilic nature and the presence of strong intra-molecular hydrogen bonding interactions drive **ERLp** to leave the ER and travel to the lysosome. Thus, the protonated conjugated imine group of **ERLp** restricts its movement in the acidic lysosomes.

In summary, a two-photon fluorescent organic probe (**ERLp**) was designed and synthesized in a facile manner. **ERLp** is non-cytotoxic and photostable. It can selectively label the Endoplasmic Reticulum (ER) with a very high Pearson colocalization coefficient of 0.91. **ERLp** can monitor ER dynamic changes during ER stress and cell apoptosis. The probe uptake by the cells' mechanistic pathway was discussed. Further, **ERLp** was confirmed to be exhibiting excellent two-photon fluorescence properties (excitation 740 nm) for studying intracellular vesicle transport from the ER to the lysosome in living cells. More importantly, the two-photon ability of **ERLp** was further explored by employing 3D multicellular tumor spheroids similar to *in vivo* tumors. Thus, **ERLp** may serve as a potential tool for monitoring ER stress or vesicle trafficking associated with pathological disorders.

The authors are grateful to the Sophisticated Instrumentation Centre (SIC), IIT Indore, for providing characterization facilities. PK is thankful to MHRD, New Delhi, for a fellowship, SKV is grateful to SERB for providing a National Postdoctoral Fellowship and SMM is thankful to SERB-DST (Project No. EMR/2016/001113), New Delhi, Govt of India and IIT Indore for financial support. The authors are thankful to Dr Ravinder Kumar for his support in confocal imaging.

Conflicts of interest

There are no conflicts to declare.

Notes and references

1 (*a*) J. M. Meinig, L. Fu and B. R. Peterson, *Angew. Chem., Int. Ed.*, 2015, **54**, 9696; (*b*) E. A. Dawidowicz, *Annu. Rev. Biochem.*, 1987, **56**, 43.
2 A. R. English and G. K. Voeltz, *Cold Spring Harbor Perspect. Biol.*, 2013, **5**, a013227.
3 D. H. Kim and I. Hwang, *Traffic*, 2013, **14**, 613.
4 C. Hetz and B. Mollereau, *Nat. Rev. Neurosci.*, 2014, **15**, 233.
5 A. Kulkarni, P. Caporali, A. Dolas, S. Johny, S. Goyal, J. Dragotto, A. Macone, R. Jayaraman and M. T. Fiorenza, *Sci. Rep.*, 2018, **8**, 9547.
6 N. Araya, Y. Takahashi, M. Shimono, T. Fukuda, M. Kato, M. Nakashima, N. Matsumoto and H. Saitsu, *Hum. Genome Var.*, 2018, **5**, 16.
7 H. Dastsooz, M. Alipour, S. Mohammadi, F. Kamgarpour, F. Dehghanian and M. Fardaei, *Hum. Genome Var.*, 2018, **5**, 18003.
8 K. Halbleib, K. Pesek, R. Covino, H. F. Hofbauer, D. Wunnicke, I. Hanelt, G. Hummer and R. Ernst, *Mol. Cell*, 2017, **67**, 673.
9 (*a*) W. Lin and B. Popko, *Nat. Neurosci.*, 2009, **12**, 379; (*b*) I. Kim, W. Xu and J. C. Reed, *Nat. Rev. Drug Discovery*, 2008, **7**, 1013.
10 (*a*) J. Colston, R. W. Horobin, F. Rashid-Doubell, J. Pediani and K. K. Johal, *Biotech. Histochem.*, 2003, **78**, 323; (*b*) L. Cole, D. Davies, G. J. Hyde and A. E. Ashford, *J. Microsc.*, 2000, **197**, 239; (*c*) M. Terasaki, Labeling of the Endoplasmic Reticulum with $DiOC_6(3)$, in Cell Biology, *A Laboratory Handbook*, ed. J. E. Celis, Academic Press, San Diego, 2nd edn, 1998, pp. 501–506.
11 (*a*) M. Terasaki and T. S. Reese, *J. Cell Sci.*, 1992, **101**(pt 2), 315; (*b*) T. Zou, C. N. Lok, Y. M. Fung and C. M. Che, *Chem. Commun.*, 2013, **49**, 5423; (*c*) J. S. Nam, M. G. Kang, J. Kang, S. Y. Park, S. J. Lee, H. T. Kim, J. K. Seo, O. H. Kwon, M. H. Lim, H. W. Rhee and T. H. Kwon, *J. Am. Chem. Soc.*, 2016, **138**, 10968.
12 M. Chalfie, Y. Tu, G. Euskirchen, W. W. Ward and D. C. Prasher, *Science*, 1994, **263**, 802.
13 H. S. Liu, M. S. Jan, C. K. Chou, P. H. Chen and N. J. Ke, *Biochem. Biophys. Res. Commun.*, 1999, **260**, 712.
14 M. A. Hoogenkamp, W. Crielaard and B. P. Krom, *J. Microbiol. Methods*, 2015, **115**, 57.
15 B. Kalyanaraman and J. Zielonka, *Redox Biol.*, 2017, **12**, 755.
16 (*a*) L. He, C. P. Tan, R. R. Ye, Y. Z. Zhao, Y. H. Liu, Q. Zhao, L. N. Ji and Z. W. Mao, *Angew. Chem., Int. Ed.*, 2014, **53**, 12137; (*b*) H. W. Lee, M. K. Cho, H. R. Kim, C. S. Lim, C. Kang and H. M. Kim, *Chem. Commun.*, 2017, **53**, 6097.
17 (*a*) H. Zhang, J. Fan, H. Dong, S. Zhang, W. Xu, J. Wang, P. Gao and X. Peng, *J. Mater. Chem. B*, 2013, **1**, 5450; (*b*) Y. Liu, C.-N. Lok, B. C.-B. Ko, T. Y.-T. Shum, M.-K. Wong and C.-M. Che, *Org. Lett.*, 2010, **12**, 1420; (*c*) S. K. Verma, P. Kumari, S. N. Ansari, M. O. Ansari, D. Deori and S. M. Mobin, *Dalton Trans.*, 2018, **47**, 15646.
18 G. Sheldrick, *Acta Crystallogr., Sect. C: Struct. Chem.*, 2015, **71**, 3.
19 P. Kumari, S. K. Verma and S. M. Mobin, *Chem. Commun.*, 2018, **54**, 539.
20 S. Huang, R. Han, Q. Zhuang, L. Du, H. Jia, Y. Liu and Y. Liu, *Biosens. Bioelectron.*, 2015, **71**, 313.
21 L. Zhu, W. Lv, S. Liu, H. Yan, Q. Zhao and W. Huang, *Chem. Commun.*, 2013, **49**, 10638.
22 (*a*) W. Lin, D. Buccella and S. J. Lippard, *J. Am. Chem. Soc.*, 2013, **135**, 13512; (*b*) H. R. Kim, R. Kumar, W. Kim, J. H. Lee, M. Suh, A. Sharma, C. H. Kim, C. Kang and J. Seung Kim, *Chem. Commun.*, 2016, **52**, 7134; (*c*) L. Kong, L. Yang, G.-B. Zhang, Q.-Y. Chen, H. Wang, X.-P. Gan, H. Li, H.-P. Zhou, J.-X. Yang and Y.-P. Tian, *J. Mater. Sci.*, 2018, **53**, 921.
23 (*a*) E. Szegezdi, S. E. Logue, A. M. Gorman and A. Samali, *EMBO Rep.*, 2006, **7**, 880; (*b*) C. M. Oslowski and F. Urano, *Methods Enzymol.*, 2011, **490**, 71.
24 H. D. Herce, A. E. Garcia and M. C. Cardoso, *J. Am. Chem. Soc.*, 2014, **136**, 17459.